ISSN 0208-7774 TRIBOLOGIA 5/2018 p. 53–64

Roksana MUZYKA[*], Piotr DUDA[**], Zbigniew ROBAK[*], Sławomir KAPTACZ[**], Sabina DREWNIAK[***]

TRIBOLOGICAL PROPERTIES OF GRAPHENE OXIDE-METAL-CARBON COMPOSITES

WŁAŚCIWOŚCI TRIBOLOGICZNE KOMPOZYTÓW TLENEK GRAFENU-METAL

Key words: rGO, Cu-C composites, surface texture, tribological properties.

Abstract

Cu-C composites are materials used for the production of brushes, contacts, and pressing shoes for electric machines due to their mechanical and wear properties. These characteristics include good thermal and electrical conductivity, a low coefficient of friction, and lubricity under varying operating conditions. Currently, graphite and copper nanopowder based materials are used as a metal-carbon material in different ratios of these components. Graphite content in this kind of material has a positive effect on the smaller consumption of, e.g., rings and commutators. In contrast, a material without graphite content is used at high current densities. The examples of such machines are a DC motor starter or generators for electrolysis characterized by large current and low voltage.

The present study tested the effect of graphene oxide (rGO) content on tribological properties in contact with steel in Cu-C composites. Tests were conducted on a ball-on-disk apparatus in conditions of dry friction. Disk wear and surface geometrical structure parameters (SGP) of the samples after tribological tests were determined on the basis of measurements made on the Talysurf.3D contact profilometer from Taylor Hobson. Damage mechanisms were identified and their relationships with structural characteristics were deducted. The hardness of Cu-C materials was higher than in copper. Cu-C based materials produce a better improvement of wear resistance, while the wear resistance of the graphene oxide based composites also decreased.

Słowa kluczowe: rGO, kompozyt Cu-C, tekstura powierzchni, właściwości tribologiczne.

Streszczenie

Kompozyty Cu-C są materiałami używanymi do produkcji szczotek, styków i ślizgów do maszyn elektrycznych ze względu na ich dobre właściwości mechaniczne i odporność na zużycie. Cechy te obejmują dobre przewodnictwo cieplne i elektryczne, niski współczynnik tarcia i samosmarność w różnych warunkach roboczych. Obecnie grafit i nanoproszek na bazie miedzi są stosowane jako materiały kompozytowe metal–węgiel w różnych proporcjach. Obecność grafitu w tym rodzaju materiału ma pozytywny wpływ na mniejsze zużycie np. pierścienia i komutatora. Materiały bez dodatku grafitu na ogół są stosowane podczas używania dużych gęstości prądu. Przykładami takich maszyn są rozrusznik silnika prądu stałego lub generatory do elektrolizy charakteryzujące się dużym prądem i niskim napięciem.

W niniejszym artykule zbadano wpływ zawartości tlenku grafenu (rGO) w kompozytach Cu-C na właściwości tribologiczne w kontakcie ze stalą. Testy przeprowadzono na urządzeniu z kula–tarcza w warunkach tarcia technicznie suchego. Zużycie tarcz i parametry struktury geometrycznej powierzchni (SGP) próbek po testach tribologicznych wyznaczono na podstawie pomiarów wykonanych na profilografometrze stykowym Talysurf 3D firmy Taylor Hobson. Zidentyfikowano mechanizmy uszkodzeń i powiązano z cechami strukturalnymi. Twardość materiałów Cu-C była wyższa niż w miedzi. Materiały na bazie Cu-C odznaczały się poprawą odporności na zużycie, podobnie jak kompozyty modyfikowane tlenkiem grafenu w porównaniu z materiałem osnowy.

[*] Institute for Chemical Processing of Coal, ul. Zamkowa 1, 41-803 Zabrze, Poland.
[**] University of Silesia, Department of Materials Science, ul. Będzińska 39, 41-200 Sosnowiec, Poland.
[***] Silesian University of Technology, Department of Optoelectronics, ul. Krzywoustego 2, 44-100 Gliwice, Poland.

INTRODUCTION

The performance of many composites, usually in terms of strength and hardness, may be enhanced by the presence of extremely small and uniformed dispersed particles or carbon materials within the original phase matrix [**L. 6**].

The electrical, energy, and electronic markets determine the use of new Cu-C composites (where graphite, soot graphite, carbon nanotubes, graphene oxide or glassy carbon are used as carbon), which are responsible for thermal conductivity and high electrical, corrosion, mechanical strength, and hydrogen resistance [**L. 1, 5, 12**].

Copper has a well-known set of basic properties (excellent electrical and thermal conductivity), but when used in abrasive composite materials, it belongs to the group of enhancers and is used in the form of fibres and powder. It affects both the mechanical strength of alloying or composites materials and, at the same time, a temperature decrease in the contact area, which are connected indirectly with good thermal conductivity properties, because there are large differences in the densities of copper and added carbon materials, which lead to their segregation [**L. 5, 7, 18**]. In the process of composite manufacturing, the type of raw materials used and the degree of their dispersing/granulation in the whole volume as well as the way of combining the ingredients are of great importance [**L. 1, 5, 14**]. The discovery of new carbon forms – graphene and graphene oxide – allows one to investigate how the addition of nanocarbon will increase the useful properties of existing composites materials. Constructing metal composites that contain carbon particles poses technological problems, due to their poor wettability and the lack of interaction with the matrix. Internal stresses are generated during production, which result from mechanical and thermal differences in the properties of the used raw materials [**L. 1, 5, 14**]. In Reference [**L. 13**], the authors presented the advantages of these composites, namely the following:

- An increase of electrical conductivity (about 10%) of copper–carbon composites vs. pure copper [**L. 13, 15**];
- An increase of about 15% in the electrical conductivity of a copper–carbon composite [**L. 13, 17**]; and,
- Increases in the hardness of 10 to 70% for various combinations of Cu powder, which were deposited with graphite, graphene and carbon nanofibers [**L. 11, 13**].

In this paper, research results of density, hardness, electrical conductivity, and tribological properties of obtained Cu-C composites were shown.

EXPERIMENTAL

Carbon Materials – Preparation of Graphite Oxide and Graphene Oxide

The commercial synthetic graphite powder (<20 μm) supplied by SGL Carbon (Nowy Sącz, Poland) (La-49 nm, Lc-27 nm, d002-0.337 nm and Cdaf-99.6%) was used as the starting sample and oxidized according to the methodology described in **Table 1**.

Table 1. Reaction conditions for the preparation of graphite oxide
Tabela 1. Warunki reakcji dla przygotowania tlenku grafitu

Sample	Reactants	Reaction time	Reference
GrO	Graphite (1g); H_2SO_4 (30mL); $NaNO_3$ (3g); $KMnO_4$ (3g)	2 h	(Ref 11)

A concentrated H_2SO_4 solution (95%–97%) was used as an acid. $KMnO_4$ and $NaNO_3$ were slowly added to keep the temperature in the 10–15°C range. After their addition, the reaction temperature was maintained between 10 and 20°C. After each reaction, the obtained mixture was dissolved in 120 mL of milli-Q water and slowly added 50 mL of 3% H_2O_2. The reaction mixture was stirred for 30 min and the mixture was centrifuged (5000 rpm for 15 min), the supernatant being decanted away. The remaining solid material was then washed with 1000 mL of water and centrifuged again, with this process being repeated until the pH was neutral. When required, GrO was dried under vacuum at 50°C overnight and stored in the presence of P_2O_5 as desiccant. Graphene oxide (rGO – thermally reduction and exfoliation) was obtained from graphite oxide by thermal treatment at 900°C in a vertical furnace, under a nitrogen flow of 50 mL/min. The residence time at the final temperature was 5 min.

Applied Measurement Methods

Both graphite oxide (GrO) and graphene oxide (rGO) possess unique properties that differ from one another to the introduction of oxygen into the sp2 bonded carbon network. We used a combination of several measurement methods to reveal the structural difference [**L. 3**].

The topography of the surface of graphite oxide and graphene oxide was investigated by means of Scanning Electron Microscopy (SEM) and Atomic Force Microscopy (AFM). For measurements using Scanning Electron Microscopy, an INSPECT S50 (FEI, Hillsboro, Oregon, USA) instrument was used. The measurement parameters were HV = 5 kV, bias = 0, spot = 3.0 and HV = 2 kV, bias = 1400 V, spot = 3.5 for graphite oxide and graphene oxide, respectively. In order to illustrate both materials, an Everhart-Thornley Detector (ETD) was used. The measurements were made under high

vacuum conditions (1.19 × 10−5 mbar). The microscope magnification was 50000×.

The results obtained by applying SEM microscopy were supplemented by the results from AFM microscopy. Investigations using this technique were performed on an N_TEGRA Prima platform (NT-MDT, Moscow, Russia) using the intermittent contact mode. The images were obtained at a resonance frequency equal to 136.281 kHz, both for graphite oxide and graphene oxide. The HA_NC tip was used in those measurements. Moreover, the Raman Spectroscopy (RS), X-ray Diffraction (XRD), and X-ray Photoelectron Microscopy (XPS) were also applied for the characterization of the layers. The Raman spectra were obtained from the N_TEGRA Spectra platform (NT-MDT). In the measurements, the wavelength was equal to 532 nm. The spectra were recorded with a resolution of 2.89 cm^{-1}.

XRD measurements were taken with an X'Pert PRO PW 3040/60 by PANalytical B.V. (Quebec, Canada) diffractometer. Samples of ground graphite, graphite oxide, and thermally reduced graphene oxide were deposited onto glass and analysed by using Co $K_{\alpha 1}$ radiation with a voltage of 40 kV and a current of 30 mA.

The elements present in graphite oxide and graphene oxide and their chemical states were identified by XPS analysis. X-ray Photoelectron Microscopy was carried out using a PHI 5000 VersaProbe – Scanning ESCA Microprobe™ (ULVAC-PHI Chigasaki, Kanagawa, Japan/Chanhassen, Minnesota, USA) and a monochrome Al Kα source (1486.6eV). The charging of the sample was corrected applying the C1s peak at 284.5eV as an internal standard. Curve fitting of the spectra was performed using a Gaussian-Lorentzian peak shape after conducting a Shirley background correction. The high-resolution C1s signal was deconvoluted into five individual peaks ascribed to graphitic carbon (284.5eV), carbon atoms with sp3 hybridization (285.4eV), hydroxyl and epoxy groups (286.5eV), carbonyl or quinone groups (287.6eV), carboxyl groups (288.9eV), and a satellite peak corresponding to the π–π* transition in the aromatic systems (290.4eV).

Composites Materials – Preparation of composites

Tribological and stereometric tests were carried out on a copper, graphene oxide - copper - graphite material. Composites were based on the following:

- Dendritic copper with a grain size of approx. 40μm (Cu + 0% rGO); and,
- carbon composites that are a mixture of dry feed consisted of 83% dendritic copper with a grain size of approx. 40 μm and 17% graphite with a grain size of approx. 60 μm and included 0 (sample base), 0.5 and 1% of rGO, respectively WSZ + 0% rGO, WSZ + 0.5% rGO and WSZ + 1.0% rGO.

Samples with rGO were mixed in a static mixer with the remaining amount of base for about 3–4 hours and then transferred into the hydraulic press mould. These prepared mouldings were sintered at max. 800°C using soot as backfill.

Applied Measurement Methods of Composites

For the obtained composite samples, bulk density, resistivity, and Shore hardness were determined. The results are given in **Table 3**. The hardness was measured using the Shore method due to the plasticity of the obtained materials.

A T-01 apparatus, ball-on-disk type, was used in order to carry out tribological tests. Tribological characteristics were recorded under conditions of dry friction with the following parameters: slip of 0.1m/s, load of 10N, friction distance of 1000m. The diameter of the friction track amounted to 24mm. AlSI 52100 steel balls (EN 100Cr6, PN ŁH15, DIN 1.3505) with a diameter of 10 mm were the tribological partner material. Room conditions were maintained in accordance with the recommendations of the VAMAS technical note [**L. 16**]: humidity – 50±10%, the ambient temperature – 23±1°C.

The intensity of the volume consumption of the samples (disk) and geometrical structure parameters of the SGP surface of the samples after tribological tests were determined on the basis of 3D measurements made on the Talysurf Series II contact profilometer from Taylor Hobson. Surface microscopic analysis of composites was performed using images taken with the Hitachi SU 70 electron microscope with a field emission together with the Thermo Scientific X-ray microanalysis system, on which EDS analyses were conducted.

RESULTS AND DISCUSSION

Characterization of the Structures – Topography and Composition of Graphite and Graphene Oxides

Figure 1 shows the photos obtained by using Scanning Electron Microscopy (magnification of 50 000 times), concerning both graphite oxide and graphene oxide.

Graphite oxide layers are quite undulating, which can attest to the fact that, during the oxidation process, surfaces have been deformed, but they were not accompanied by interruption of their continuity. The structure of graphite oxide is smoother than that of graphene oxide; moreover, it displays a parallel arrangement of the respective layers (**Fig. 1**).

The results of tests carried out when applying Atomic Force Microscopy confirm the difference in the development of these structures. The topography (2×2 μm) of the surface of graphene oxide is presented in **Fig. 3**. The topography of graphite oxide changes within a larger range (from 0 to 170 nm) than that of graphene oxide (from 0 to 11 nm). Analysing the cross-sections (**Figs. 2b** and **3b**) across the surface (marked by the blue lines in **Figs. 2a** and **3a**), we see that, with both materials, the changes in height amount

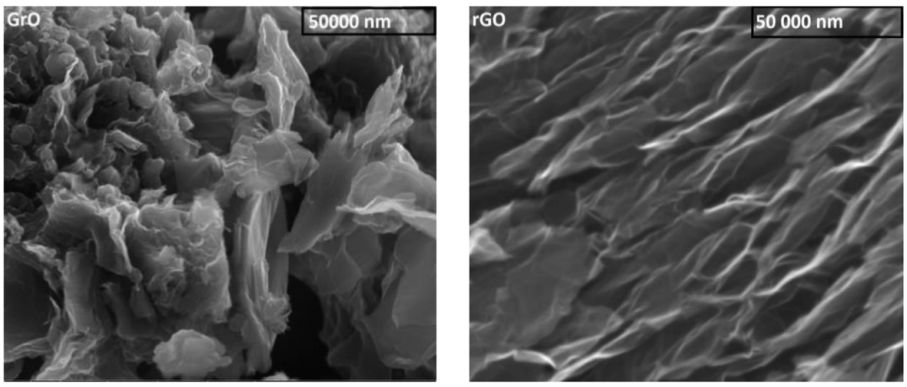

Fig. 1. Photos of structures obtained by using Scanning Electron Microscopy (magnification of × 50 000): structure with graphite oxide and graphene oxide

Rys. 1. Zdjęcia struktur uzyskanych za pomocą skaningowej mikroskopii elektronowej (powiększenie × 50 000): struktury z tlenkiem grafitu i tlenkiem grafenu

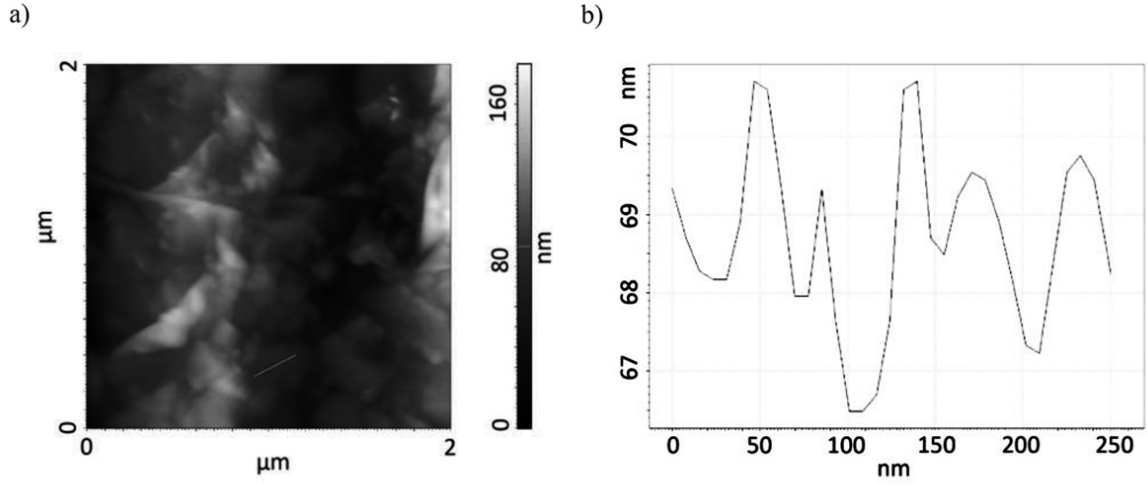

Fig. 2. Topography of the surface of graphite oxide: (a) picture obtained by using AFM, (b) cross-sections of the marked area

Rys. 2. Topografia powierzchni tlenku grafitu: (a) obraz uzyskany za pomocą AFM, (b) przekrój zaznaczonego obszaru

to several nanometres along the cross-section of 250 nm (GrO) and 1.5 µm (rGO). The resulting graphite oxide thickness is about 70 nm, and the graphene oxide thickness is about 5 nm. The value of the RMS coefficient for graphite oxide amounts to RMS = 15.98 nm, whereas, for graphene oxide, it amounts to RMS = 0.52 nm, which proves the better development and smoothness of the surface of graphene oxide.

The crystalline structures of synthesized graphite oxide and graphene oxide, as well as that of graphite, were analysed by XRD. As shown in **Fig. 4**, the XRD pattern of the graphite shows a diffraction peak at 2Θ = 30.80°, corresponding to its interlayer spacing (d002) of 0.3369 nm. The intensity of this peak sharply decreases for GrO, and a new 001 peak appears at 2Θ = 13.37°. The d001 interlayer distance calculated for this sample is 0.7687 nm, which is in agreement with its high degree of oxidation [**L. 4**]. The variation in the interlayer spacing of GrO results in the variation in the degree of oxidation on graphite and is proportional to the content of oxygen. Apart from the characteristic sharp diffraction peak at 2Θ = approximately 13°, the mildly oxidised rGO exhibits another weak peak at 2Θ = 30°. In the case of the thermal reduction of GrO, the characteristic peak of GrO at 2Θ = 13.37° has been reported to disappear and a new broad peak appears at 2Θ = 30.99°. The decrease in the interlayer spacing

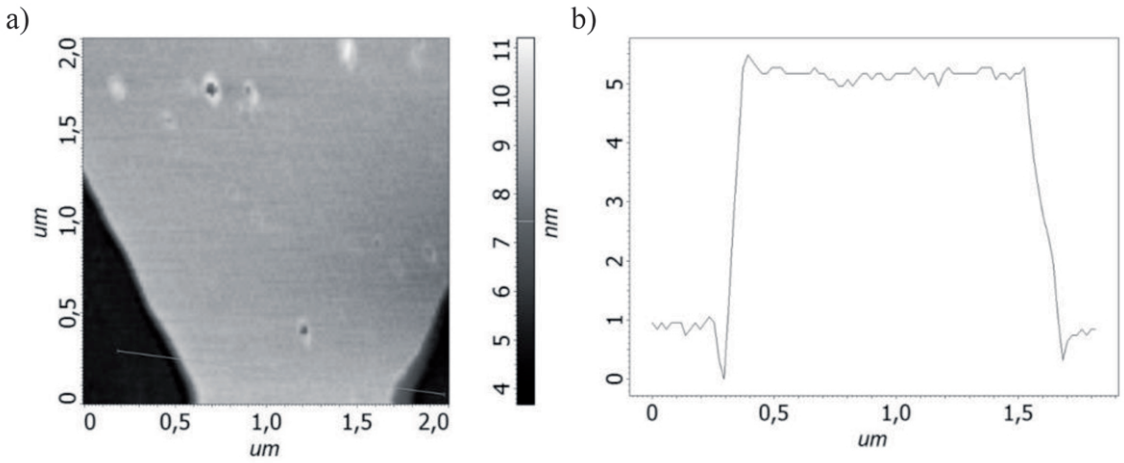

Fig. 3. Topography of the surface of graphene oxide: (a) picture obtained by using AFM, (b) cross-sections of the marked area

Rys. 3. Topografia powierzchni tlenku grafenu: (a) obraz uzyskany za pomocą AFM, (b) przekrój zaznaczonego obszaru

between the thermally reduced graphene oxide sheets is attributed to the removal of considerable oxygen functionalities from the GrO sheet during the reduction process. The interlayer spacing d002 amounts to 0.3351 nm.

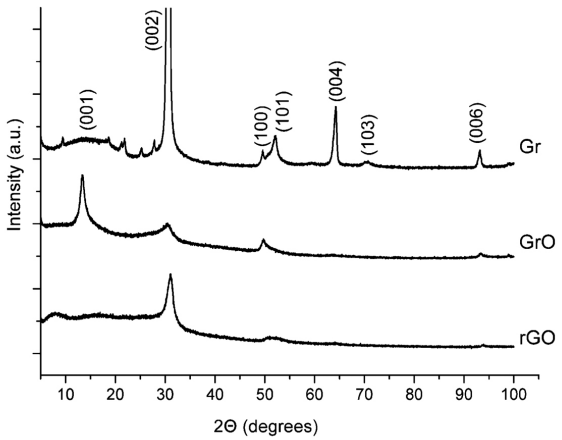

Fig. 4. X-ray patterns for the graphite, GrO and rGO treated at 900°C

Rys. 4. Dyfraktogramy rentgenowskie dla grafitu GrO i rGO w temperaturze 900°C

The oxygen speciation was studied by means of XPS measurements. **Figure 5** shows the C1s core-level XPS spectra of graphite and graphene oxides. The spectra of GrO show an intense peak at 284.5eV, attributed to carbon with sp^2 hybridization accompanied by some shoulders at higher binding energies due to the presence of oxygen linkages [**L. 4**]. The samples also show a second intense peak at 286.5eV, ascribed to hydroxyl and epoxy groups, and less intense contributions of carbonyl/quinone (287.6eV) and carboxyl (288.9eV) groups. The oxygen speciation in these samples is in agreement with the model of Lerf-Klinowski concerning highly oxidized graphitic structures [**L. 4, 10**]. The spectrum of rGO shows an intense peak at 284.5 eV attributed to carbon with sp^2 hybridization. The C1s spectrum consists of a peak at 285.4, 286.2, 287.9, 288.9, and 290.4 eV assigned to Csp^3 hybridization, C–O, C=O, O=C–OH and π–π* transition in aromatic systems [**L. 9**].

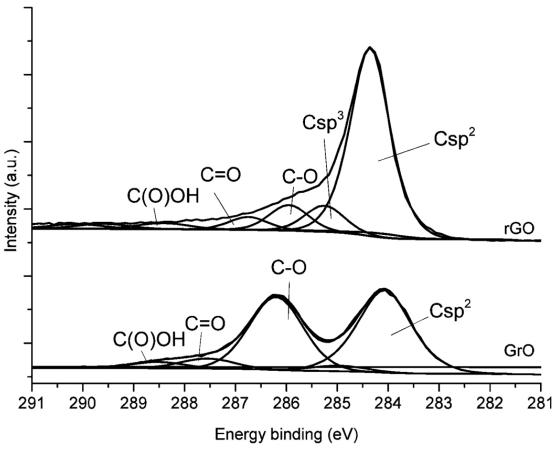

Fig. 5. Deconvolution of C1s core-level XPS spectra of the GrO and rGO

Rys. 5. Dekonwolucja widm XPS na poziomie podstawowym C1s dla GrO i rGO

The results of the deconvolution of the C1s XPS spectra are gathered in **Table 2**.

Table 2. Elemental composition of GrO and rGO determined by XPS
Tabela 2. Skład pierwiastkowy GrO i rGO określony za pomocą XPS

Sample	Elemental Composition, %		C1s Deconvolution				
	C	O	Csp^2	Csp^3	C–O	C=O	C(O)OH
GrO	70.3	29.7	51.0	0	40.0	3.3	5.7
rGO	92.0	8.0	71.7	13.3	10.6	3.9	0.5

The Raman spectra of GrO and rGO are shown in **Figure 6**. The two most intensive peaks occur in the ranges 1300–1400 cm^{-1} (D) and 1550–1600 cm^{-1} (G) [**L. 2, 4**]. The ratio of the intensities of the D and G peaks for GrO is equal to 1.01; whereas, for rGO, it equals 1.06. The growth of this ratio suggests that the amount of defects increased.

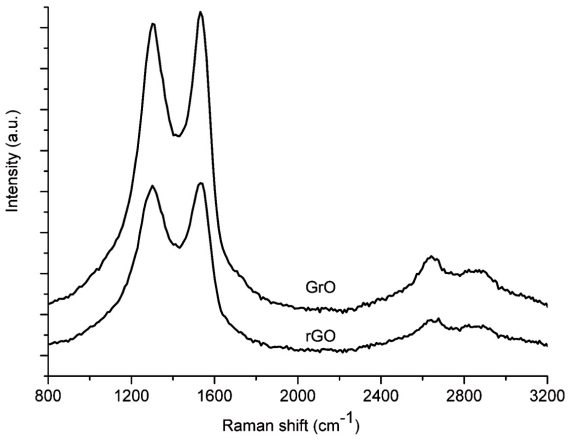

Fig. 6. Raman spectra of graphite oxide and graphene oxide
Rys. 6. Widma Ramana tlenku grafitu i tlenku grafenu

Characterization of the Composites Materials

The results are given in **Table 3**. The hardness was measured using the Shore method due to plasticity of the obtained materials.

Table 3. Characteristics of the obtained composites
Tabela 3. Charakterystyka uzyskanych kompozytów

	Bulk density [g/cm³]	Relative density 20°C	Resistivity, r 10^{-6} [Ω·m]	Shore hardness, [Sh]
Cu + 0% rGO	7.59±0.15	7.60±0.15	1.71±0.06	11±0.25
WSZ + 0% rGO	4.98±0.16	4.99±0.16	7.71±0.08	16±0.25
WSZ+ 0.5% rGO	4.91±0.16	4.92±0.16	8.91±0.08	16±0.25
WSZ + 1.0% rGO	4.80±0.16	4.81±0.16	11.76±0.10	18±0.25

Comparing the parameters of the brush material and the brush material with the content rGO of pure copper, it can be said that the relative density decreases for the brush material with and without the addition of graphene material. An inverse relationship was observed for other parameters of resistance and Shore's hardness.

Microscopic observation was performed in order to confirm the presence of rGO on the surface composite. Sample pictures of the surface prepared to cooperate with the arrangement of graphene oxide flakes are provided in **Fig. 7**. The distribution of small cavities and holes is stochastic. Flakes of rGO protruding from the composite were not noted. This reflects the large forces that occurred during the polishing process necessary to prepare the samples. The only optically visible evidence of the occurrence of graphene material was cracked pieces spread on the surface looking like a flaky shell (**Fig. 8**).

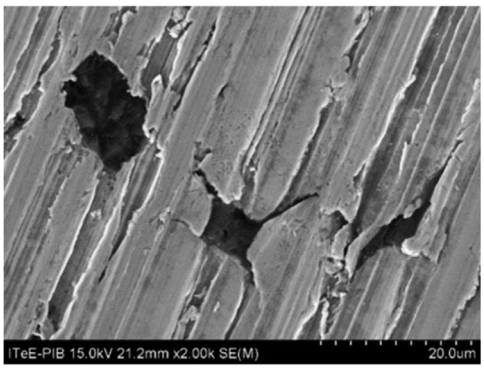

Fig. 7. SEM image of the composite surfaces with the distribution of graphene oxide particles. Visible microcraters in the matrix material
Rys. 7. Obraz SEM powierzchni kompozytowych z rozkładem cząstek tlenku grafenu. Widoczne mikrokratery w materiale osnowy

Darker places occurring randomly in **Fig. 7** are losses in matrix material. Closer observation revealed that only in a few cases of the edge composition of the particles was the copper material separation caused by the process of preparation for tribological investigations. In order to confirm the presence of graphene oxide, EDS analysis was performed on a given area. **Figure 9** shows the analysis of the sample cavity formed under the influence of the matrix material to break. The results clearly show the carbonaceous material located on the walls of the recess, and it was not observed on the surrounding surface.

The opposite situation occurs with respect to the matrix material. Copper is detected outside the cavity. Point analysis (**Fig. 10**) confirmed similar cavities in the elemental composites of the surface and the surfaces of adjacent matrix material. Studies on the matrix showed a different elemental composition and low carbon

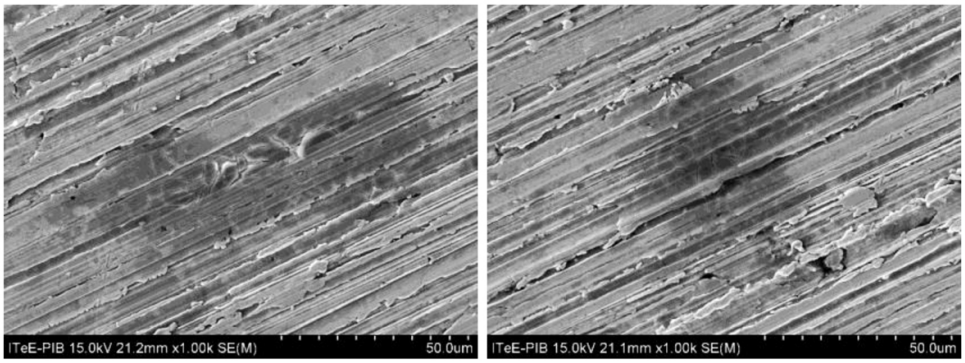

Fig. 8. SEM images of samples prepared for tribological tests. In this example, graphene oxide particles arranged parallel to the surface can be noticed

Rys. 8. Obrazy SEM próbek przygotowanych do badań tribologicznych. W tym przykładzie można zauważyć cząstki tlenku grafenu rozmieszczone równolegle do powierzchni

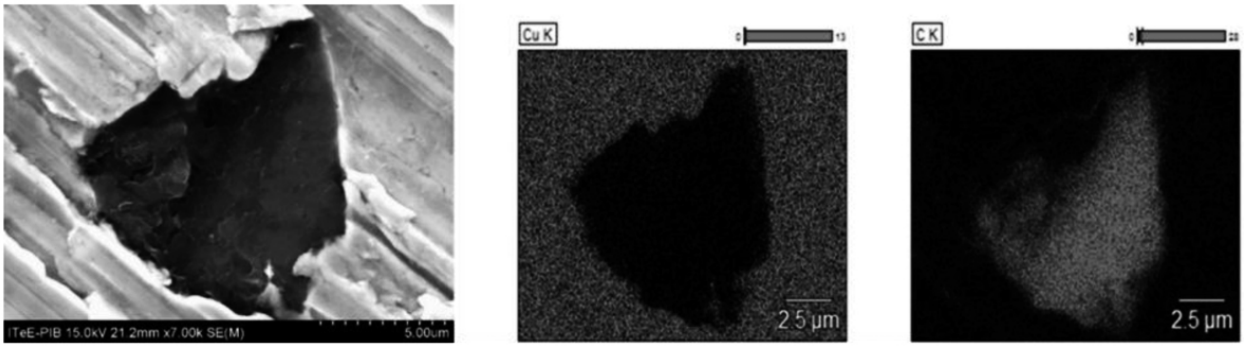

Fig. 9. Distribution of copper and carbon elements in the hole

Rys. 9. Rozkład pierwiastków miedzi i węgla w otworze

a)

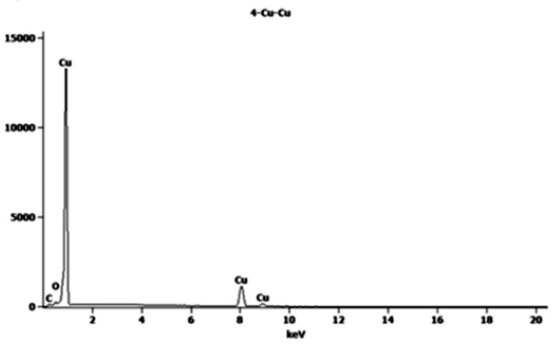

Element Line	Weight %
C K	1.70
O K	0.81
Cu K	97.48

b)

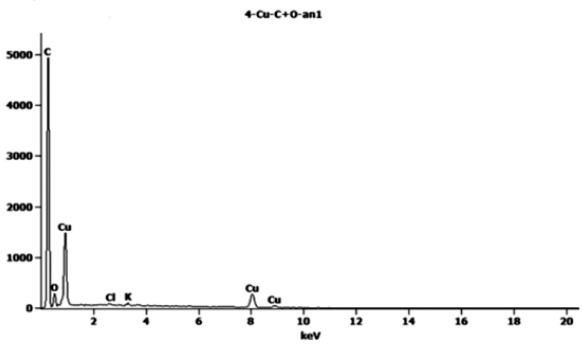

Element Line	Weight %
C K	54.02
O K	5.79
Cl K	0.67
K K	0.71
Cu K	38.82

Fig. 10. Analysis of the elemental composition a) on the matrix material surface, b) on the side surface of the hole

Rys. 10. Analiza składu pierwiastkowego a) na powierzchni materiału osnowy, b) na bocznej powierzchni otworu

content (**Fig. 10a**). A large share of carbon and oxygen and a small share of copper were characteristic of the surface depressions.

The research of the geometric structure of the surface (SGP) was carried out before tribological tests to determine the status of the surface preparation and afterwards to determine the width of the path of friction. We analysed mainly the amplitude parameters.

On the graphical visualization of Sa (arithmetic mean deviation of the surface), Sq (root-mean-square deviation of the surface), and Sp (maximum height of summits) parameters (**Fig. 11**), significant differences (that exceed to 20% of the value between analysed samples) are not observed. Only in the case of the brush material (WSZ) containing 0.5% of rGO was there a greater value Sp with respect to the base material (WSZ). Pure copper was used as a reference. Test surface prepared from pure copper has significantly lower values of the Sa and Sq, and the parameter Sp is lower than the base metal by more than 30%. This demonstrates a significantly smoother surface and a significantly lower impact on the tops of the individual state.

Analysing other parameters, e.g., Sv (maximum depth of valleys), St.(total height of the surface), and Sz (ten point height of the surface), gives rise to close conclusions concerning the previously analysed parameters (**Fig. 12**). The parameters Sp and St are strongly correlated, and this dependence is also observed in the present case. By comparing the parameters of the brush material and the brush material with the content of pure copper rGO, we can say that the surface roughness and thus the maximum depth of the recesses and the height of the peaks of the reference material (copper material) are significantly lower. It is not caused by the process of preparing the surface, since the procedure was identical.

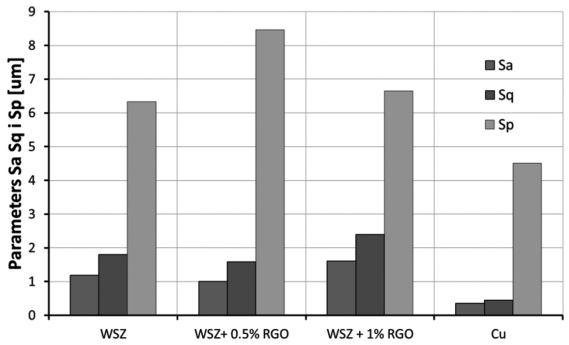

Fig. 11. Characterization of the material surfaces. Surface parameters Sa, Sq and Sp

Rys. 11. Charakterystyka powierzchni materiałów. Parametry powierzchni Sa, Sq i Sp

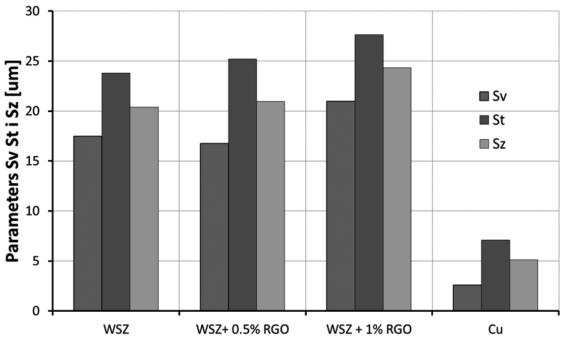

Fig. 12. Characterization of the material surfaces. Surface parameters Sv, St and Sz

Rys. 12. Charakterystyka powierzchni materiałów. Parametry powierzchni Sv, St i Sz

Amplitude parameters are strongly correlated to better determine the condition of the surface prior to testing tribological further analysed parameters Ssk (skewness of the topography height distribution) and Sku (kurtosis of the topography height distribution) [**L. 8**]. They are sensitive to the peaks and valleys, showing the exact shape information of the test surface. Ssk with a value below zero and large values of Sku the brush material and the brush for the product modified petals rGO testify to the smooth surface of the flat tops and small dominant recesses (**Fig. 13**). Another image of the reference material is copper, which has a smooth surface with sharp slopes. The results indicate that the geometric structure of the surface of the base material of the brush and brush-modified product of 0.5% and 1% rGO do not significantly differ among themselves, but they are different in comparison with to the reference material surface, which is to shield from dendritic copper.

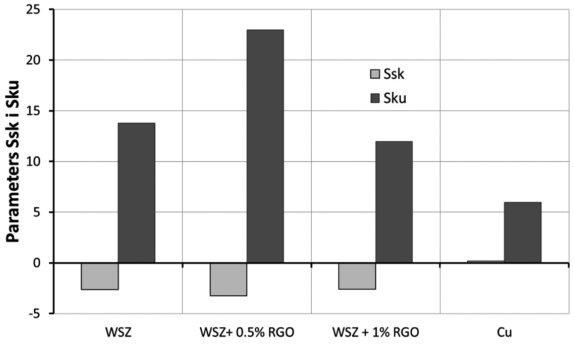

Fig. 13. Characterization of the material surfaces. Surface parameters Ssk and Sku

Rys. 13. Charakterystyka powierzchni materiałów. Parametry powierzchni Ssk i Sku

In order to determine the changes in the tribological characteristics under the influence of material modification of the brush by the introduction of reduced graphene oxide thermally, tribological studies on ball-on-disk tester were conducted. Samples after the

first series of tribological measurements are shown in **Fig. 14**. The clear friction paths on the disks surfaces and low wear observed on the surface of steel ball (AISI 52100) surfaces prove substantially lower wear resistance for the abrasive brush material and copper dendritic partner of tribological material.

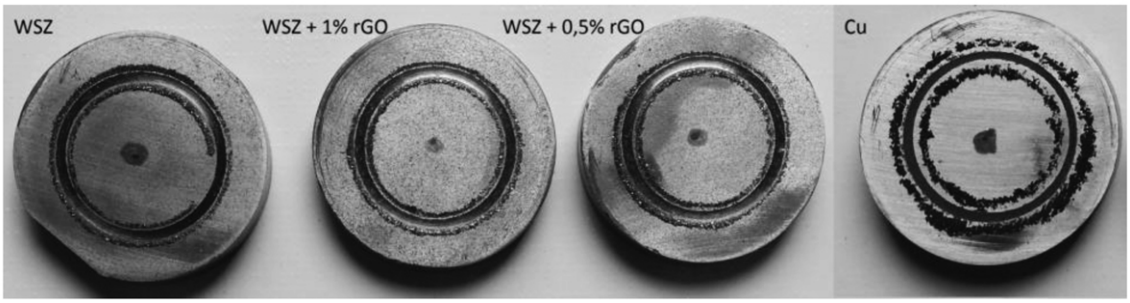

Fig. 14. Disks after the 1st phase of tribological measurements
Fig. 14. Wygląd tarcz po pierwszej fazie testów tribologicznych

The longitudinal track cooperation located on beads (**Fig. 15**) and their mass consumption not registered confirm that the material sensitive nodes in this type of friction material are copper-based. The state of the surface of composites after tribological cooperation is shown in **Fig. 16**.

Characteristics consumables of the disks material were determined by friction track width measurements at least 10 locations perpendicular to the trace paths. Exemplary measurement is showed in **Fig. 17**. When analysing the track width of each friction material, it can be said that they have little scatter compared to the reference material (**Fig. 18**). The width of the friction path, which is characterized by the intensity of wear of target material, has very significant differences between the various materials. Only about 30% of the variation of copper dendritic indicates that the product has a more predictable brush wear intensity, and thus it is easier to predict the service life of the friction material which uses a brush and brush material modified cereal rGO.

Fig. 15. Disk and ball after a tribological test (example)
Rys. 15. Tarcza i kulka po teście tribologicznym (przykład)

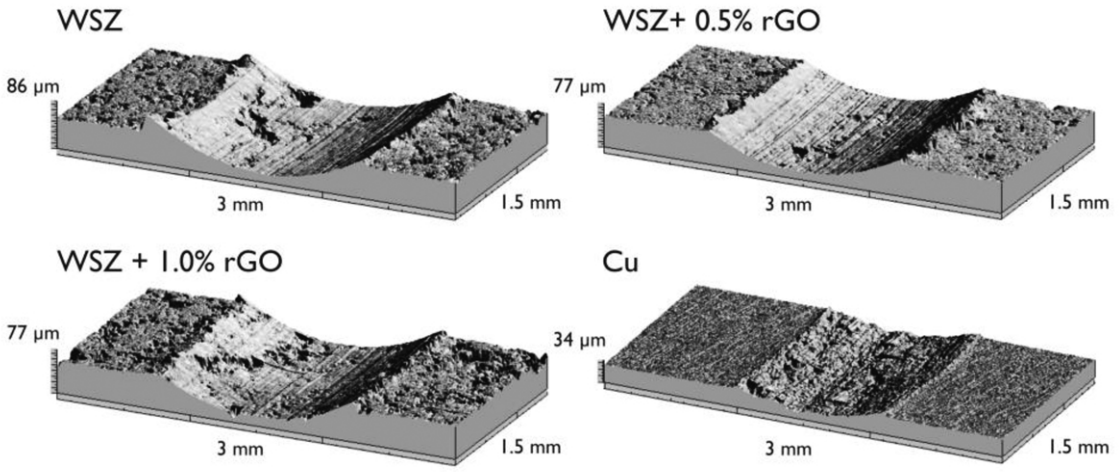

Fig. 16. The surface condition of composites after tribological cooperation
Rys. 16. Stan powierzchni kompozytów po współpracy tribologicznej

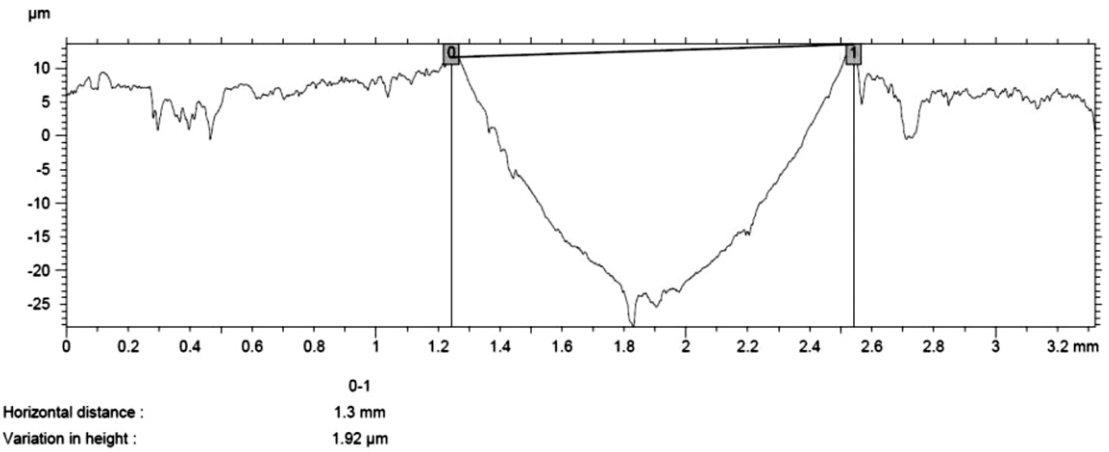

Fig. 17. Measurement of the wear path width (method explanation)
Rys. 17. Pomiar szerokości ścieżki zużycia (wyjaśnienie metody)

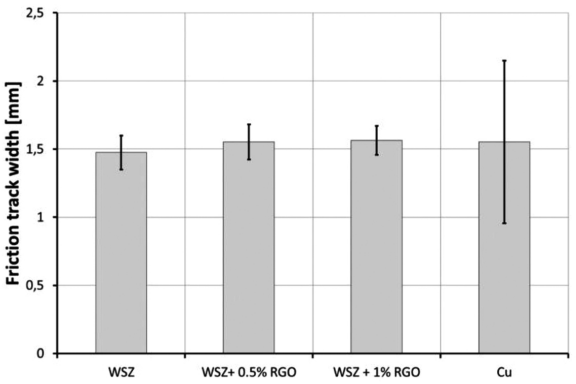

Fig. 18. Friction track width depending on the material type
Rys. 18. Szerokość śladu współpracy w zależności od rodzaju materiału tarczy

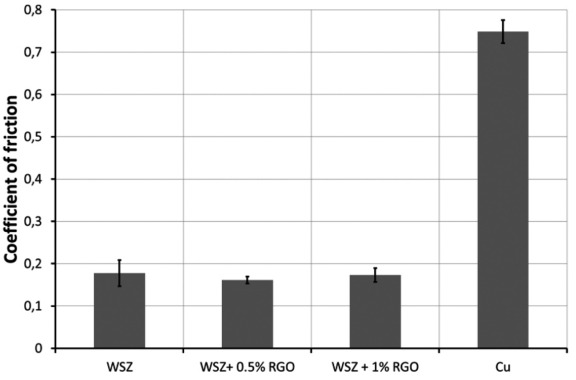

Fig. 19. Coefficient of friction for the all tested couples (mean values)
Rys. 19. Współczynnik tarcia dla wszystkich badanych par (wartości średnie)

Since the brush material already contained graphite in its composition, which is grease, the modification of thermally reduced graphene oxide had no significant impact on the value of the coefficient of friction stabilized (**Fig. 19**). Tribological pairs from the article brush and modified rGO were characterized by almost a fourth of the coefficient of friction compared to the base material together with steel balls. That conclusion is to analyse the characteristics of the friction force sample tests as a function of time (**Fig. 20**). For the shell material of the brush device, the friction force is at 1.8 N; whereas, in the case of copper dendritic, the friction value has a very unstable course and is at a level above 7 N.

CONSLUSIONS

The composites based on brush material and thermally reduced graphene oxide presented in this paper are characterized by the stochastic distribution of the reinforcing material flakes. It is this characteristic structure that causes, during surface preparation, plucking of the matrix material fragments contained between the graphene oxide and the material surface. EDS analysis confirms the presence of the carbonaceous material on the walls of the holes in the material surface and on the technically prepared top layer.

The geometric structure of the top layer of brushes of all materials is similar, which the analysed amplitude parameters confirm. Further analysis of the parameters indicates that the composites have a surface with clear periodicity of traces. In the case of the base material - dendritic copper, it can be said that the sample surface is smooth with flat peaks and small dominant cavities.

The tribological tests performed under standardized parameters have shown that the material brush-based

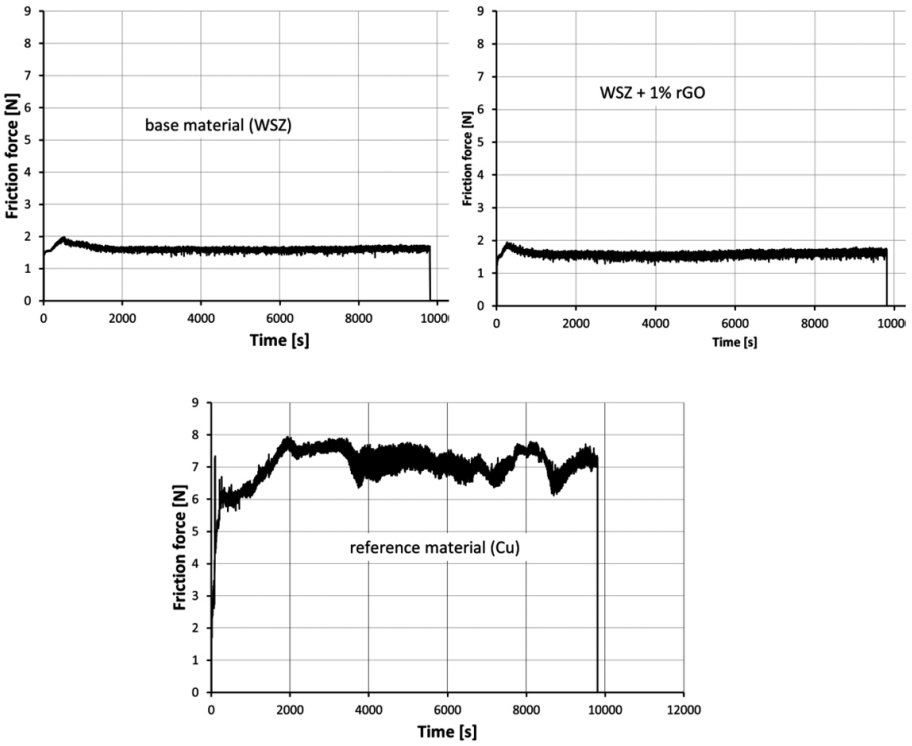

Fig. 20. Characteristics of the friction force for the base material, WSZ + 1% of rGO and reference material as a function of cooperation time

Rys. 20. Charakterystyka siły tarcia dla materiału bazowego, WSZ + 1% rGO i materiału odniesienia w funkcji czasu współpracy

composites modified by the addition of 0.5 and 1% of rGO have a coefficient of friction that is almost one-third of that for the matrix material without reinforcement. Unfortunately, the intensity of shield material wear changes to the disadvantage of the composites – dendritic copper. For the rGO content of 0.5%, there is even slightly greater width of the cooperation trace. The reduction of the coefficient of friction and maintenance of the similar wear intensity are obtained in the case of the composite containing 1% of rGO.

Brush material as a product has a more predictable wear intensity and thus it is easier to predict the service life of the friction material which uses a brush and brush material modified flake rGO.

REFERENCES

1. Chmielewski M., Dutkiewicz J., Mańkowska-Snopczyńska A., Michalczewski R., Pietrzak K.: 'The method of tribotesting of PVD coated elements in oscillatory motion at high temperatures', Tribologia, 2014, No. 5, pp. 45–57, in Polish.
2. Drewniak S., Pustelny T., Muzyka R., Konieczny G., Kałużyński P.: 'The effect of oxidation and reduction processes of graphite on physicochemical properties of graphite oxide and reduced graphene oxide', Photonics Lett. Pol., 2014, Vol. 6, No. 4, pp. 130–132.
3. Drewniak S., Pustelny T., Muzyka R., Plis A.: 'Studies of physicochemical properties of graphite oxide and thermally exfoliated/reduced graphene oxide', Pol. J. Chem. Tech., 2015, Vol. 17, No. 4, pp. 109–114.
4. Drewniak S., Muzyka R., Stolarczyk A., Pustelny T., Kotyczka-Morańska M., Setkiewicz M.: 'Studies of Reduced Graphene Oxide and Graphite Oxide in the Aspect of Their Possible Application in Gas Sensors', Sensors, 2016, Vol. 16, No. 103, pp. 16010103.
5. Duda P., Muzyka R., Robak Z., Kaptacz S.: 'Mechanical Properties of Graphene Oxide–Copper Composites', Archives of Metallurgy and Materials, 2016. Vol. 61, No. 2, pp. 863–868.

6. Hvizdoš P., Besterci M., Ballóková B.: 'Tribolical behaviour and mechanical properties of copper and magnesium based composites treatment by severe plastic deformation', Int. J. of Materials and Product Technology, 2015, Vol. 50, No. 1, pp. 80–100.
7. Juszczyk B., Kulasa J., Malara S., Czepelak M., Malec W., Cwolek B., Wierzbicki Ł.: 'Tribological Properties of Copper-Based Composites with Lubricating Phase Particles', Archives of Metallurgy and Materials, 2014, Vol. 59, No. 1, pp. 615–620.
8. Kacalak W., Lipiński D., Tomkowski R.: 'Podstawy jakościowej oceny stanu powierzchni kształtowanych z wykorzystaniem teorii zbiorów rozmytych', Pomiary, Automatyka, Kontrola, 2008, Vol. 54, pp. 180–183, in Polish.
9. Kaniyoor A., Imran Jafri R., Arockiadoss T., Ramaprabhu S.: 'Nanostructured Pt decorated graphene and multi-walled carbon nanotube based room temperature hydrogen gas sensor', Nanoscale, 2009, Vol. 1, pp. 382–386.
10. Ko G., Kim H.Y., Ahn J., Park Y.M., Lee K.Y., Kim J.: 'Graphene-based nitrogen dioxide gas sensors', Curr. Appl. Phys., 2010, Vol. 10, No. 3, pp. 1002–1004.
11. Koltsova T.S., Nasibulina L.I., Anoshkin I.V., Mishin V.V., Kauppinen E.I., Tolochko O.V., Nasibulin A.G.: 'New Hybrid Copper Composite Materials Based on Carbon Nanostructures', J. Mater. Sci. Eng., 2012, No 2, pp. 240–246.
12. Knych T., Smyrak B., Walkowicz M.: 'Charakterystyka cech materiałowych i technologicznych miedzi beztlenowej dedykowanej do aplikacji kablowych', Rudy i Metale Nieżelazne, 2012, Vol. 57, No. 4, pp. 250–257, in Polish.
13. Knych T., Kwaśniewski P., Kisiewicz G., Mamala A., Kawecki A., Smyrak B.: 'Characterization of Nanocarbon Copper Composites Manufactured in Metallurgical Synthesis Process', Metallurgical and Materials Transactions B, 2014. Vol. 45, No. 4, pp. 1196–1203.
14. Myalski J.: Monografia. Kształtowanie właściwości tribologicznych kompozytów zawierających węgiel szklisty. Wydawnictwo Politechniki Śląskiej, in Polish, 2011.
15. Nayfeh T.H., Wiederholt A.M.: Patent US, 2012, No. 0152480.
16. Piekoszewski W., Tuszyński W., Szczerek M., Wiśniewski M.: 'Testowanie tarcia i zużycia materiałów ceramicznych i stali w ramach programu VAMAS', Tribologia, 1994, Vol. 138, pp. 716–728, in Polish.
17. Shugart J.V., Scherer R.C.: Patent. US, 2010, No. 0327233 A1.
18. Wojciechowski A., Gołowicz A., Michalski R.: 'Influence of the form of copper in the friction material of disc brakes on the coefficient of friction and wear in rig tests', The Archives of Automotive Engineering, 2013, Vol. 62, pp. 77–88, in Polish.